A benchmark natural rubber-based elastocaloric refrigerator

Álvaro Juliá Maroto
Faculty of Physics, University of Barcelona, Diagonal 645, 08028 Barcelona, Spain.

Advisor: Dr. Enric Stern Taulats

Abstract:
Natural rubber (NR) is a cheap and accessible polymer that presents a giant caloric response to applied tensions due to stress-driven crystallisation. The reversibility of the process can be exploited to implement a refrigeration device that uses the material's symmetric caloric response under periodically applied/released tension to cool it below room temperature, acting as a heat sink. In this thesis, NR's adiabatic temperature change ΔT_{ad} under applied stress is studied subjecting samples to different tensions within an 80-120 N range and observing their temperature evolution via infrared imaging. The mechanical work required to induce the crystallisation is also calculated in order to derive NR's coefficient of performance COP_{NR} with and without energy recovery conditions, for comparison. The results indicated that a 90 N tension (3.35 MPa in strain) provided optimised caloric response without compromising the sample's resistance. A simple device was then designed to test the effectiveness of NR as a refrigerant for cooling a water heat exchanger circuit, aimed to serve as a model for comparison for upgraded cooling prototypes. Temperature evolution during the cooler's operation was registered using thermocouples for 20 consecutive cycles, yielding an effective cooling of $\Delta T_{span} = 0.65 \pm 0.05$ K after 400 seconds, resulting in a performance coefficient for the device of $COP_p = 0.36 \pm 0.02$, and an effective cooling power per refrigerant mass of $P_p = 4.1 \pm 0.2$ W kg^{-1}.

I. INTRODUCTION

Mechanocaloric materials present a large entropy variation due to stress-induced ordering, which implies a giant caloric response. These materials are classified as either barocaloric, twistocaloric, elastocaloric, etc., depending on the particular symmetry of the stress field responsible for the effect [1]. Elastocaloric materials, which present caloric effects when the applied force field is uniaxial, show great potential as an alternative to the conventional vapour-compression cooling technology [2]. Despite the fact that shape-memory alloys have been the most promising candidates so far [3], recent NR-based cooling prototypes have achieved effective refrigeration of 1.5-1.9 K [4].

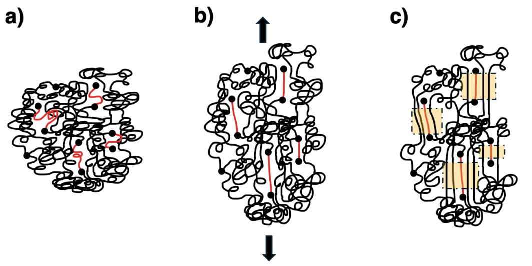

FIG. 1: Schematic of crystallisation process responsible for elastocaloric effect on a NR sample under tensile stress. (a) High entropy relaxed state, (b) Elongation under applied tension, (c) Crystallisation-driven entropy reduction. Polymer chains align forming crystallites (yellow regions).

Natural rubber (NR) has elastocaloric properties that have been known for centuries [5]. The caloric effect in NR originates from the strain-induced crystallisation latent heat, resulting from the significant reordering of individual polymer chain segments into clusters known as crystallites, as shown in Figure 1, adapted from [6]. The material's elastocaloric behaviour can be described through the thermodynamic variables $(T, S, \varepsilon, \sigma)$, corresponding to temperature, entropy, and strain and Cauchy stress tensors respectively (taken as scalars for simplicity while working within the uniaxial constraint). A Brayton cycle was designed, as shown in Figure 2, that allows NR to be implemented as a refrigerant.

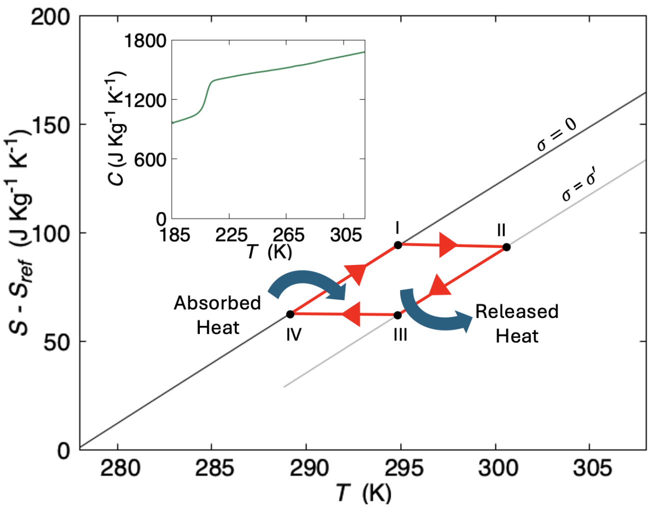

FIG. 2: Brayton cycle of NR chosen for prototype implementation, consisting on two adiabatic stages $(I-II\ ,III-IV)$ and two isofield thermalisations $(II-III\ ,IV-I)$. Inset represents NR's heat capacity as a function of temperature.

The presented entropy variation curve at zero field was obtained integrating the equation $dS = C\ dT/T$, yielding $S - S_{ref} = \int_{T_{ref}}^{T} C dT/T$, where T_{ref} is an arbitrary reference temperature, S_{ref} is its corresponding reference entropy, and C is the heat capacity, measured beforehand and presented as an inset in Figure 2. The curve for $\sigma = \sigma'$ is obtained by shifting the first curve by an amount in T, which corresponds to the adiabatic temperature change of the material under applied stress ΔT_{ad}, assumed to be constant over this temperature range [7]. When subjected to the cycle as a refrigerant, NR absorbs heat through thermal contact during the cold zero-field stage (IV-I), and releases it through thermalisation during the (II-III) isofield segment.

II. EXPERIMENTAL METHODS

Figure 3 presents the two distinct setups used. Panel (a) shows the experimental setup used to characterise NR's elastocaloric performance, discussed in section III.A, and panel (b) illustrates the design and implementation of the prototype, discussed in section III.B.

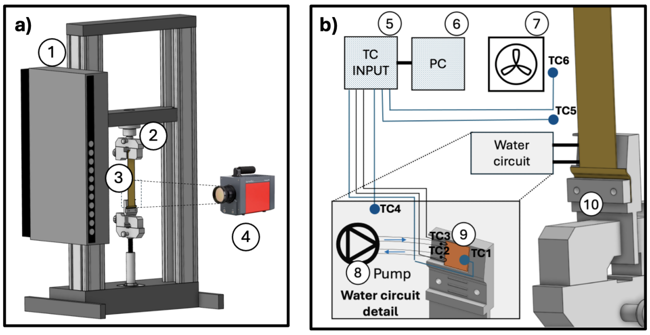

FIG. 3: Experimental setup for refrigerant characterisation(a) and prototype (b). **(1)** Zwick-Roell mechanical testing machine, **(2)** 500 N load cell, **(3)** Commercial NR sample, **(4)** Infrared camera, **(5)** Thermocouple interface connected to 6 thermocouples. TC 2,3 are fine-gauge K-types and the rest are J-Types, **(6)** Computer for data acquisition via LabView, **(7)** Fan to favour thermalisation of the sample when crystallised, **(8)** Copper heat exchanger, **(9)** Water pump, **(10)** Custom-made grip.

To characterise the refrigerant, a 3.67 g sample of commercial vulcanised NR was cut into a dog-bone shape to prevent extreme tensions along sample borders from a sheet of 1.2 mm of thickness and with a square exposed area of 4.84 cm^2, just like the heat exchanger used in the prototype, in order to maximise effective thermal contact. These were then mounted on a Zwick-Roell Z005 Mechanical testing machine and subjected to several elongation cycles at 5 cm s^{-1}. Force-strain measurements were acquired through a Zwick-Roell X-Force HP load cell with a 500 N threshold and a sensitivity of 2 mV V^{-1}. Data collection and test parameter control were both achieved through Zwick-Roell's software, TextXpert II. NR's heat capacity was also obtained using modulated calorimetry on a 21.07 mg sample via a DSC Q2000 from TA Instruments, with a modulation amplitude of $\pm$ 0.5 K and a period of 60 s.

Cycles started with a pre-load of 10 N, and then the sample was stretched to a set force threshold. Tests were force-controlled instead of position-controlled to eliminate the effects of deformation from the sample in each iteration, which would produce bends and prevent the IR camera from producing focused images [8]. The temperature variations of the samples were observed throughout the 10 cycles using an InfraTec IR Image 8800 thermographic camera, which recorded high-resolution imaging of the sample registering a temperature value for each pixel at 25 fps. These data were later treated using the Irbis Professional 3.1 software to obtain temperature profiles and estimate ΔT_{ad}.

As shown in Figure 3(b), the prototype required a water circuit and a copper heat exchanger (HE) to be mounted on the custom-made grips, whose design maintained the HE in a fixed position at a 5º angle away from the sample with respect to its vertical axis, along which the force was applied. This allowed the NR to make good thermal contact with the HE when contracted, and pulled it away when stretched. A pump was operated at a minimum voltage of $3V$ and water was pumped through the HE only during its contact with the cold NR, to minimise pump heat contributions. A non-silicon thermal paste was used to aid thermal contact between NR and HE, and the circuit's tubes were covered in insulating foam to minimise thermal losses. A fan was implemented to ensure faster sample thermalisation.

During prototype operation, temperatures were monitored using 6 thermocouples (TC), connected to a 16-channel 24 bit USB-9162 National Instruments TC interface. TC4, TC5 and TC6 (J-Type) registered ambient temperatures around the pump, sample and fan areas respectively. TC1 (J-Type) was put in contact with the HE. TC2 and TC3 (fine gauge, K-type) were inserted in the HE's output and input tubes, respectively, to directly measure incoming/outcoming water temperature.

III. RESULTS AND DISCUSSION

A. Refrigerant characterisation

Figure 4 presents the experimental results of the stress and thermographic tests conducted on NR samples to observe their adiabatic temperature change. Samples were first subjected to a training in order to minimise the impact of the Mullins effect [9].

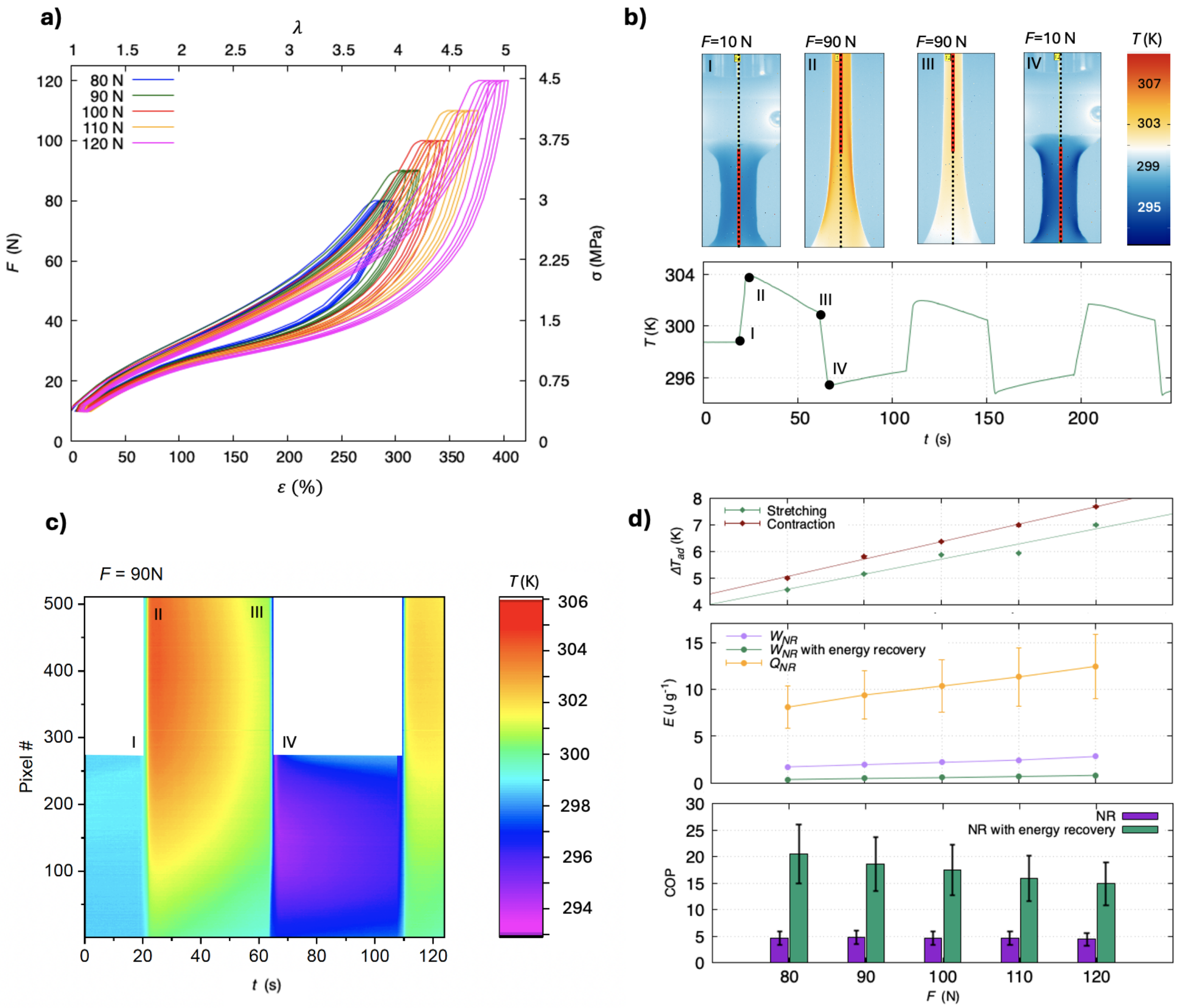

FIG. 4: (a) Force-strain curves for series of 5 cycles between 10 N and a varying maximum force. Auxiliary axis for uniaxial stress σ and relative elongation have been added. (b) Top images: Thermographic images of the sample at stages I through IV of the Brayton cycle. Dashed lines indicate the chosen temperature profile used in characterisation, and red lines indicate the particular selected data for determining temperature at each stage of the cycles, to avoid gradients and non-sample values. Bottom diagram: The averaged temperature from the selected red profiles over time. (c) Temperature-time contour diagram of the complete vertical dashed profile presented in panel (b) throughout one cycle, for a more apparent representation of the sample's temperature gradients. The contributions from the grip when the sample is contracted have been excluded and are indicated by the white areas. (d) Temperature increment and energetic characterisation as a function of maximum applied force. Top diagram: adiabatic temperature change estimated as temperature increment between I and II (green line) or II and IV (red line). Errors are statistically obtained and not visible. Central diagram: line plot of energy contributions per unit mass of NR: Mechanical work with and without energy recovery, and maximum estimated exchangeable heat for the samples. Bottom diagram: Bar plot of NR's coefficient of performance with and without energy recovery conditions.

After training the material, sets of 5 cycles were performed, starting at 10 N, then stretching to a varying force threshold and holding for 40 seconds in both cases to allow thermalisation. The sample's stretching and contraction were performed rapidly to ensure adiabaticity. Panel (a) displays force-strain curves for various maximum force values, where the auxiliary axis λ, is the relative elongation. The process recreates the Brayton cycle previously depicted in Figure 2. The stages are labelled accordingly (I-IV), and shown at each corresponding instant in Figure 4(b) and (c), for the 90 N test. The cycle was repeated to check the reproducibility needed for prototype functionality, but the material was characterised using data from the first cycle only.

Temperature during each thermodynamic process was estimated by averaging IR camera pixel values along the central dashed vertical line in Figure 4(b), which spans 511 pixels. During stages I and IV, the sample was fully visualised by the camera so temperature was estimated as the average of values along the lower 255 pixel segment, in red. In stages II and III, however, samples present inhomogeneous stress distributions along their edges and base, resulting in significant temperature gradients. To avoid them, temperature is instead averaged along the upper 256 pixels. Panels (b) and (c) show the estimated temperature evolution over the first three cycles for the 90 N cycles.

The temperature change values ΔT_{ad}, for both the adiabatic stretching and contraction, were calculated as $T_{II} - T_I$ and $T_{III} - T_{IV}$, respectively. This analysis is repeated for the first cycle of all five tested forces obtaining the values presented on the upper diagram in panel (d), which present proportionality to the applied stress. It is worth noting that technical limitations of the camera's maximum field of view do not allow direct observation of the full stretched sample, particularly the centre where stress (and thus, temperature increment) is maximised, which implies $T_{II,III}$ are underestimates. $T_{I,IV}$, on the other hand, are overestimated due to incomplete thermalisation, which prevents the rubber from cooling to the extent that it could theoretically achieve after contracting. These two error sources imply that all obtained ΔT_{ad} are underestimates and thus, only the higher values corresponding to the contraction data set will be used in the following calculations.

To characterise the material's caloric performance for each employed maximum force, values for the mechanical work W_{NR} and potentially exchangeable heat Q_{NR} were determined and presented in the central diagram of panel (d). W_{NR} required to crystallise is calculated by integrating the upper envelope of the first force-strain cycle shown in panel (a). W_{NR} values considering energy recovery are calculated as the area of the hysteresis cycle instead. Systems with energy recovery, where the elastic potential energy gained by the material during its elongation is used to assist an asynchronous sample's stretching process, are significantly more efficient due to the greatly reduced energetic requirement. Maximum potentially exchangeable heat is estimated as $Q_{NR} = C_{NR}\Delta T_{ad}$, considering NR's heat capacity as $C_{NR} = 1.62$ J g^{-1} K^{-1}, constant within the experimental range (see Figure 2 inset). The material's coefficient of performance (COP) is defined as the ratio between maximum exchangeable heat and mechanical work. It is presented in the inferior diagram on panel (d) considering both standard cycling and energy recovery, to showcase the vast benefits of the latter. Other studies have also shown similar values and that the COP decreases as applied stress increases, due to significant increments in the dissipated energy through hysteresis [10].

B. Prototype performance

The previous data suggested that the the optimal operation force for the refrigerator would be 90 N, to prevent breaks. Thus, 10-90 N cycles were employed with a hold time of 15 seconds, which offered adequate fan-assisted thermalisation and thermal contact times for prototype functionality.

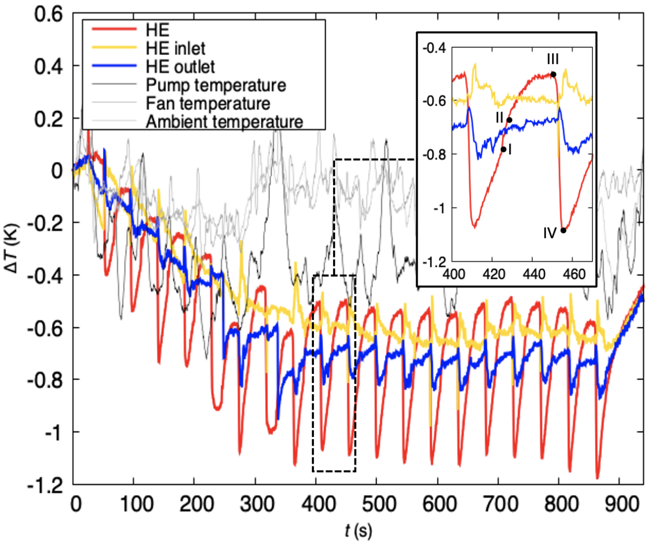

FIG. 5: Variation in temperature registered by thermocouples during device operation with 10-90 N cycles and hold times of 15 seconds. 20 consecutive cycles are performed reaching a temperature reduction $\Delta T_{span} = 0.65 \pm 0.05$ K at 400 seconds (9 cycles), where the device reaches a stationary state. Inset offers a detailed vision of one cycle, depicting each stage of the Brayton cycle along the heat exchanger temperature curve. Room temperature values (Gray lines) are also presented for reference.

The device described in Figure 3(b) operated for 20 consecutive cycles registering water, HE and ambient temperature via the thermocouples. Figure 5 shows the temperature variations of the different sensors with respect to their initial values. The pump was activated only during the cold phase of the cycles (IV-I) where the sample absorbed heat from the circuit. Otherwise, it remained inactive to minimise heating. A fan was used to assist thermalisation during the hot phases (I-III) and thus, increase cycling frequency. Note that a small temperature difference between the HE inlet and outlet is always present due to pump heating and thermal losses.

Temperatures reached a stationary region after 400 seconds where the thermal losses and gains were compensated, halting refrigeration. The effective temperature reduction at this point was $\Delta T_{span} = 0.65 \pm 0.05$ K, estimated as the average between heat exchanger inlet and outlet temperatures at 400 s. Considering the refrigeration of both the water ($m = 1.06$ g, with a heat capacity of 4.14 J g^{-1} K^{-1}) and the copper HE

(m = 12.32 g, and heat capacity 0.39 J g^{-1} K^{-1}), the cooler extracted a total heat of 5.9 ± 0.3 J.

The prototype's coefficient of performance is defined here as the ratio between total extracted heat and total mechanical work before reaching stationary conditions, considering strictly the energy recovery work, previously calculated as the area of the hysteresis cycle (9 cycles for a total of 16.7 J), yielding $COP_p = 0.36 \pm 0.02$. To improve this value, it is important to reduce losses that limit the ΔT_{span} through enhanced thermal insulation and prevention of unwanted thermal contact between NR and HE, since the simplicity of this design has the downside of having no moving parts to allow the NR to be completely removed from the exchanger during the hot region of the cooling cycle. However, the grip's inclination offers enough separation to prevent total thermal contact.

On the other hand, the number of cycles required to reach the stationary state depend on the quality of the heat absorption, which can be increased by using more mass of refrigerant. For comparison purposes with future devices, the cooler's refrigeration power per refrigerant mass is defined as the ratio between the previously calculated total extracted heat and the time required to reach the stationary conditions, and is equal to $P_p = 4.1 \pm 0.2$ W Kg^{-1}. The prototype could be scaled, adding more refrigerant samples to increase its power. It is worth noting that these two quantities are minimum thresholds for this particular cooler design, since only the heat extracted to its cold region (water and HE) was considered in their calculations, and not cooling to other components.

IV. CONCLUSIONS

The results provide a characterisation of NR's caloric response in the 80-120 N maximum force range. For each tested value ΔT_{ad} was estimated, presenting proportionality to the applied stress. The potentially exchangeable heat for the samples, and the mechanical work were calculated with and without energy recovery. Results show that the material's COP is best at relatively low strains, due to the decreased mechanical work requirements for cycling and the increased sample fatigue resistance. It was observed that the material's coefficient of performance decreases when using greater stress, since mechanical work requirements increase faster than potentially exchangeable heat.

A simple refrigeration device was implemented using 10-90 N force-controlled cycles on a single NR sample, achieving an effective temperature reduction of $\Delta T_{span} = 0.65 \pm 0.05$ on a water heat exchanger circuit after 9 cycles. A stationary state was reached by the cooler preventing further refrigeration and thus, the device's performance was determined by this stationary threshold. Its performance coefficient and refrigeration power per mass of refrigerant were calculated to be $COP_p = 0.36 \pm 0.02$, and $P_p = 4.1 \pm 0.2$ W Kg^{-1}, respectively.

The simplicity of the prototype's design, although limiting with regards to its effectiveness, offers valuable information, as it can be used as a reference for more advanced NR-based refrigerator projects to compare their performances. Even without complete control of thermal contact and using only one sample the device was able to achieve effective refrigeration within reasonably short times. Any upgraded NR-based cooler should present comparably superior performance characteristics. This comparison could be of aid in estimating the impact of specific design improvements on overall machine effectiveness, aiding in elastocaloric cooling technology development towards commercialisation.

Acknowledgements

I want to thank my advisor, Dr. Enric Stern for his guidance and dedication, my laboratory colleague Toni Vives for his assistance in addressing experimental complications and custom grip fabrication, and Dr. Eduard Vives for his insight and discussion. Very special thanks to my family and my friends, whose opinion and company have been my motor throughout the development of this thesis.

[1] How, H., Quian, S., Takeuchi, I. *Nat. Rev. Mat.* **7** 641 (2022)
[2] Goetzler, W., Zogg, R., Young, J., Johnson, C. Energy savings potential and RD & D opportunities for non-vapor-compression HVAC. 16-22 (2014).
[3] Junyu, C., Lei, L., Fang, G. *Mater. Today Commun.* **28** 3 (2021)
[4] Sion, M. et al. *J. Phys. Energy* **6** 8 (2024)
[5] Gough, J. *Mem. Lit. Phil. Soc. Manchester.* **1** 288–295 (1805).
[6] Tosaka, M. et al. *Macromol.* **37** 3306 (2004)
[7] Xie, Z., Sebald, G., Guyomar,D. *Phys. Lett. A* **381** 2114 (2017)
[8] Bonnot, E., Romero, R., Mañosa, L., Vives, E., Planes, A. *Phys. Rev. Lett.* **100** 2 (2008)
[9] Diani, J., Fayolle, B., Gilormini, P. *Eur. Polym. J.* **45** 602-604 (2009)
[10] Sebald, G., Lombardi, G., Coativy, G., Jay, J., Lebrun, L., Komiya, A. *Appl. Therm. Eng.* **223** 3,8 (2023)